arXiv:gr-qc/0505113v1 23 May 2005

Perturbative Analysis of Universality and Individuality in Gravitational Waves from Neutron Stars

L.K. Tsui and P.T. Leung[1]

Physics Department and Institute of Theoretical Physics,
The Chinese University of Hong Kong,
Shatin, Hong Kong SAR, China.

February 7, 2008

ABSTRACT

The universality observed in gravitational wave spectra of non-rotating neutron stars is analyzed here. We show that the universality in the axial oscillation mode can be reproduced with a simple stellar model, namely the centrifugal barrier approximation (CBA), which captures the essence of the Tolman VII model of compact stars. Through the establishment of scaled co-ordinate logarithmic perturbation theory (SCLPT), we are able to explain and quantitatively predict such universal behavior. In addition, quasi-normal modes of individual neutron stars characterized by different equations of state can be obtained from those of CBA with SCLPT.

Subject headings: gravitational waves — stars: neutron — stars: oscillations (including pulsations) — equation of state — relativity

1. Introduction

As is well known, neutron stars of high densities are ideal extra-terrestrial test beds for theories of nuclear matters, quark matters and high energy physics (see e.g. Glendenning 1997, and references therein). For instance, the possible existence of the quark star (see e.g. Cheng et al. 1998), a variant of the neutron star, could lend direct support to the theory of quark matter (Chodos et al. 1974; Witten 1984; Alcock et al. 1986; Prakash et al. 1990). Besides, the relation between the mass and the radius of a neutron star could determine,

[1]Email: ptleung@phy.cuhk.edu.hk

up to certain accuracy, the equation of state (EOS) of relevant nuclear matter through the process of inversion (Lindblom 1992). Therefore, a comprehensive study of observed data and statistics of neutron stars is likely to lead to fruitful results in the fields mentioned above.

Traditional means to gather information about neutron stars have so far relied on electromagnetic waves emitted from them. However, with the advent of gravitational wave detectors of various designs (see e.g. Hughes 2003; Mason 2004, and references therein), including resonant antennas (e.g. EXPLOPER and NIBOE), ground-based interferometers (e.g. LIGO and VIRGO), and the space-based interferometer LISA, it is generally believed that neutron stars, as promising gravitational wave emitters, can be observed and analyzed in the gravitational wave channel within one or two decades. For example, it has been argued that the frequency of detection of gravitational waves emitted in the mergers of binary neutron stars could be as high as several hundreds per year in the near future (Belczynski et al. 2001; Hughes 2003). Besides, gravitational waves could also be emitted during the formation of neutron stars (Lindblom et al. 1998; Fryer et al. 2002). Being spurred on by the possibility of inferring the internal structure of neutron stars from the gravitational wave signals emitted by them, researchers have been actively examining the peculiarities embedded in such signals (Andersson & Kokkotas 1996, 1998; Benhar et al. 1999; Kokkotas et al. 2001).

Despite that the evaluation of gravitational waves emitted in violent stellar activities such as binary mergers and asymmetric core collapse has indeed posed a grand challenge to researchers in numerical relativity, linearized theory of pulsating neutron stars pioneered by Thorne & Campolattaro (1967) can still provide useful insight into such complex situations. By analogy of radiating electric circuits (Kokkotas & Schutz 1986), linearized gravitational waves are analyzed in terms of quasi-normal modes (QNMs), which are damped harmonic pulsations with time dependence $\exp(\mathrm{i}\omega t)$ and are characterized by complex eigenfrequencies $\omega = \omega_{\mathrm{r}} + \mathrm{i}\omega_{\mathrm{i}}$ (Press 1971; Leaver 1986a; Ching et al. 1996; Kokkotas & Schmidt 1999; Nollert 1999). It is believed that the QNM frequencies of a pulsating neutron star can reflect the physical characteristics of the star, such as its mass M, radius R and EOS as well (Andersson & Kokkotas 1996, 1998; Benhar et al. 1999; Kokkotas et al. 2001). However, Andersson & Kokkotas (1998) and Benhar et al. (1999) also noted that the frequency ω_{r} and the damping time $\tau \equiv 1/\omega_{\mathrm{i}}$ of the leading axial and polar w-modes of non-rotating neutron stars follow approximately the equations:

$$\omega_{\mathrm{r}} \approx \frac{1}{R}\left[a_{\mathrm{r}}\left(\frac{M}{R}\right) + b_{\mathrm{r}}\right], \tag{1-1}$$

$$\frac{1}{\tau} \approx \frac{1}{M}\left[a_{\mathrm{i}}\left(\frac{M}{R}\right)^2 + b_{\mathrm{i}}\left(\frac{M}{R}\right) + c_{\mathrm{i}}\right], \tag{1-2}$$

where $a_{\rm r}$, $b_{\rm r}$, $a_{\rm i}$, $b_{\rm i}$ and $c_{\rm i}$ are model-independent constants determined from curve fitting. These universal behaviors seem to undermine the possibility of inferring the characteristics of a neutron star from its w-mode QNMs. Instead, they are indicative of a common feature shared among neutron stars with different EOS's.

To seek the physical mechanism underlying the universality in the gravitational wave of neutron stars, we showed in a recent paper (Tsui & Leung 2004) that (i) The scaled complex eigenfrequencies $\tilde{\omega} \equiv M\omega$ of w-mode oscillations, to a good approximation, depend only on the compactness $\mathcal{C} \equiv M/R$. (ii) Eqs. (1-1) and (1-2) are equivalent to a single formula of $\tilde{\omega}$:

$$\tilde{\omega} \approx a \left(\frac{M}{R}\right)^2 + b \left(\frac{M}{R}\right) + c, \tag{1-3}$$

where a, b and c are complex constants. (iii) The universality indicated by (1-3) is a direct reflection of the fact that the the mass distribution inside neutron stars with different EOS's can be nicely approximated by the Tolman VII model (TVIIM) proposed by Tolman (1939).

In this paper we further pinpoint the crux of the mechanism leading to the universal behavior (1-3) for axial w-mode pulsations. Inspired by the success of TVIIM, we propose here yet another simple approximation, namely the centrifugal barrier approximation (CBA), in which the potential in the axial gravitational wave equation (Chandrasekhar & Ferrari 1991a) is replaced by a standard centrifugal barrier in the tortoise radius plus a constant determined from continuity of the potential at the stellar surface. The CBA potential yields the correct asymptotic behavior of the actual potential at the center of the star and is a good global approximation as well. The wave function of the axial gravitational wave equation in CBA then becomes exactly solvable. It is remarkable that the universal behavior (1-3) can still be reproduced with CBA using the tortoise radius of TVIIM star as an input. Hence, the observed universality in neutron star axial pulsations is in fact ascribable to (i) the centrifugal potential at the center of the star; (ii) the continuity of the potential; and (iii) the tortoise radius of TVIIM star, which will be given explicitly in Sect. 2 of our paper.

To understand quantitatively the universal behavior (1-3), we establish here a scaled co-ordinate logarithmic perturbation theory (SCLPT), which is a generalization of the logarithmic perturbation theory (LPT) formulated previously to study QNMs of "dirty black holes" (Leung et al. 1997, 1999). Applying SCLPT to CBA and using the tortoise radius of TVIIM star, we obtain from first principle the numerical values of a, b and c in (1-3). The universal behavior (1-3) is therefore substantiated analytically.

While the CBA star itself clearly displays universality as mentioned above, we can also obtain accurate QNM frequencies of individual realistic neutron stars from those of CBA with SCLPT. As a consequence, we are able to consider the EOS-dependence of the scaled

QNM frequency $\tilde{\omega}$ from the static structure of a star (e.g. mass distribution), thereby paving the way for inferring the EOS of a star from its gravitational wave spectra. Thus, the universality and individuality in QNMs of neutron stars constructed with different EOS's are fully explored with SCLPT developed in this paper.

The organization of our paper is as follows. In Sect. 2, after briefly reviewing the scaling behavior of the axial gravitational wave equation, we introduce CBA and show that under such approximation QNMs still manifest the generic behavior summarized in (1-3). In Sect. 3 we formulate SCLPT to study how QNM frequencies are affected by changes in the potential and the tortoise radius of the star. In Sect. 4 we apply SCLPT to expand the scaled QNM frequency $\tilde{\omega}$ as a quadratic function of the compactness of the star and in turn corroborate the universal behavior in (1-3). In Sect. 5 SCLPT is applied to investigate the EOS-dependence of the scaled QNM frequency $\tilde{\omega}$. We then conclude our paper in Sect. 6 with a discussion studying the applicability of CBA and SCLPT to $w_{\rm II}$ and trapped modes (see e.g. Kokkotas & Schmidt 1999; Chandrasekhar & Ferrari 1991b). Unless otherwise stated, geometrized units in which $G = c = 1$ are adopted in the present paper and numerical results are shown for the least damped mode of quadrupole gravitational waves.

2. Generic behavior of QNMs and CBA

The eigenvalue equation for QNMs of axial oscillations of neutron stars is given by a Regge-Wheeler-type equation (Chandrasekhar & Ferrari 1991a):

$$\left[\frac{\mathrm{d}^2}{\mathrm{d}r_*^2} + \omega^2 - V(r_*)\right]\psi(r_*) = 0. \tag{2-1}$$

Here the tortoise coordinate r_* is related to the circumferential radius r by

$$r_* = \int_0^r \mathrm{e}^{(-\nu+\lambda)/2}\mathrm{d}r, \tag{2-2}$$

where $e^{\nu(r)}$ and $e^{\lambda(r)}$ are metric coefficients defined by the line element $\mathrm{d}s$ as follows:

$$\mathrm{d}s^2 = -e^{\nu(r)}\mathrm{d}t^2 + e^{\lambda(r)}\mathrm{d}r^2 + r^2(\mathrm{d}\theta^2 + \sin^2\theta\mathrm{d}\varphi^2). \tag{2-3}$$

In addition, the metric coefficient $e^{-\lambda(r)}$ is given explicitly by:

$$e^{-\lambda(r)} = 1 - \frac{2m(r)}{r}, \tag{2-4}$$

with $m(r)$ being the mass-energy inside circumferential radius r. The potential V inside the star is given by:

$$V(r_*) = \frac{\mathrm{e}^{\nu}}{r^3}[l(l+1)r + 4\pi r^3(\rho - P) - 6m(r)], \tag{2-5}$$

where $\rho(r)$ and $P(r)$ are the mass-energy density and the pressure at a point (r, θ, φ), respectively. Outside the star, the tortoise radial coordinate reduces to

$$r_* = r + 2M \ln\left(\frac{r}{2M} - 1\right) + C, \tag{2-6}$$

where C is a constant that can be obtained by matching (2-2) with (2-6) at $r = R$, and the potential V is given by the well known Regge-Wheeler potential (Regge & Wheeler 1957).

$$V_{\rm rw}(r_*) = \left(1 - \frac{2M}{r}\right)\left[\frac{l(l+1)}{r^2} - \frac{6M}{r^3}\right]. \tag{2-7}$$

Eq. (2-1), referred to as neutron star Regge-Wheeler equation (NSRWE) in the following discussion, and the outgoing wave boundary condition at spatial infinity together determine the QNM frequency of axial w-mode oscillations. We show in Fig. 1 the QNM frequencies obtained numerically for neutron stars with different EOS's, including models A (Pandharipande 1971a) and C (Pandharipande 1971b) proposed by Pandharipande, three models (AU, UU and UT) proposed by Wiringa et al. (1988), models APR1 and APR2 proposed by Akmal et al. (1998), and model GM24 (Glendenning 1997, p. 244). It is clearly shown that both the real and imaginary parts of the scaled frequency $\tilde{\omega}$ are well approximated by quadratic functions in compactness $\mathcal{C}$, as indicated by the dotted lines in the corresponding figures. This in turn leads to the universality discussed in Sect. 1.

To investigate the physical origin underlying the universality, we have shown that the axial mode wave equation displays scaling behavior (Tsui & Leung 2004), and can be rewritten as follows:

$$\left[\frac{\mathrm{d}^2}{\mathrm{d}\tilde{r}_*^2} + \tilde{\omega}^2 - \tilde{V}(\tilde{r}_*)\right]\tilde{\psi}(\tilde{r}_*) = 0, \tag{2-8}$$

where

$$\tilde{V}(\tilde{r}_*) \equiv M^2 V(\tilde{r}_*) = \begin{cases} \mathrm{e}^{\tilde{\nu}}\tilde{r}^{-3}\left[l(l+1)\tilde{r} + 4\pi\tilde{r}^3(\tilde{\rho} - \tilde{P}) - 6\tilde{m}(\tilde{r})\right], & \tilde{r} \le R/M; \\ (1 - 2\tilde{r}^{-1})\left[l(l+1)\tilde{r}^{-2} - 6\tilde{r}^{-3}\right], & \tilde{r} > R/M; \end{cases} \tag{2-9}$$

and

$$\tilde{r} = \frac{r}{M}, \tag{2-10}$$

$$\tilde{r}_* = \frac{r_*}{M}, \tag{2-11}$$

$$\tilde{m}(\tilde{r}) = \frac{m(r)}{M}, \tag{2-12}$$

$$\tilde{P}(\tilde{r}) = M^2 P(r), \tag{2-13}$$

$$\tilde{\rho}(\tilde{r}) = M^2 \rho(r), \tag{2-14}$$

$$\tilde{\nu}(\tilde{r}) = \nu(r). \tag{2-15}$$

Besides, we also let $\tilde{R} \equiv R/M$ and $\tilde{R}_* \equiv R_*/M$, where $R_* = r_*(r = R)$ is the tortoise radius of the star.

From (2-8) it is then apparent that the mass-independence of the scaled frequency $\tilde{\omega}$ follows directly from that of the scaled potential $\tilde{V}$. Motivated by this and noting that the following mass distribution:

$$m_{\rm c}(r) = M\left[\frac{5}{2}\left(\frac{r}{R}\right)^3 - \frac{3}{2}\left(\frac{r}{R}\right)^5\right], \tag{2-16}$$

conventionally termed as TVIIM in the literature (Tolman 1939; Lattimer & Prakash 2001), is indeed a good approximation of $m(r)$ for neutron stars with various EOSs (see Fig. 2), we demonstrated that QNMs of TVIIM (solid circles in Fig. 1) display universal behavior observed in realistic stars and interpreted such universality as the consequence of the mass-independence of the scaled mass distribution of TVIIM (Tsui & Leung 2004):

$$\tilde{m}_{\rm c}(\tilde{r}) \equiv \frac{m_{\rm c}(r)}{M} = \frac{5}{2}\mathcal{C}^3\tilde{r}^3 - \frac{3}{2}\mathcal{C}^5\tilde{r}^5. \tag{2-17}$$

In addition to approximating the mass distribution in realistic neutron stars, TVIIM is a solvable model whose metric coefficients e^λ and e^ν can be obtained in closed forms (Tolman 1939):

$$e^{-\lambda} = 1 - \mathcal{C}\xi^2(5 - 3\xi^2)\ , \tag{2-18}$$

$$e^{\nu} = (1 - 5\mathcal{C}/3)\cos^2\phi\ . \tag{2-19}$$

Here $\xi = r/R$,

$$\phi = (w_1 - w)/2 + \phi_1\ , \tag{2-20}$$

$$w = \log\left[\xi^2 - \frac{5}{6} + \sqrt{\frac{e^{-\lambda}}{3\mathcal{C}}}\right], \tag{2-21}$$

$$\phi_1 = \phi(\xi^2 = 1) = \arctan\sqrt{\frac{\mathcal{C}}{3(1 - 2\mathcal{C})}}\ , \tag{2-22}$$

$$w_1 = w(\xi^2 = 1)\ , \tag{2-23}$$

and the pressure is given by:

$$P = \frac{1}{4\pi R^2}\left[\sqrt{3\mathcal{C}e^{-\lambda}}\tan\phi - \frac{\mathcal{C}}{2}(5 - 3\xi^2)\right], \tag{2-24}$$

By using (2-18), (2-19) and the definition of r_*, we obtain

$$r_* = R\int_0^\xi I(\xi', \mathcal{C})\mathrm{d}\xi', \tag{2-25}$$

where

$$I(\xi,\mathcal{C}) = \left\{\left[1-\mathcal{C}\xi^2(5-3\xi^2)\right](1-5\mathcal{C}/3)\cos^2\phi\right\}^{-1/2}. \tag{2-26}$$

Hence, the scaled tortoise radius of the star is

$$\tilde{R}_* = \frac{1}{\mathcal{C}}\int_0^1 I(\xi,\mathcal{C})\mathrm{d}\xi. \tag{2-27}$$

Since TVIIM has a mass profile similar to those of realistic neutron stars, we expect differences in $\tilde{R}_*$ between TVIIM and realistic neutron stars would be small. In fact, our conjecture is verified by Fig. 3 where R_*/M is plotted against M/R for TVIIM and other realistic stars.

As the integral in (2-25) could not be evaluated analytically, we are not able to express $V(r_*)$ in terms of simple functions of r_* and hence it is not possible to find the analytical form of the wave function in NSRWE even inside the star. However, we could expand $V(r_*)$ as a power series around the center of the star:

$$\tilde{V}(\tilde{r}_*) = \frac{l(l+1)}{\tilde{r}_*^2} + \tilde{\alpha} + O(\tilde{r}_*^2), \tag{2-28}$$

where $\tilde{\alpha}$ is a constant dependent on $\mathcal{C}$ and l. It is worthwhile to note that the leading term in the expansion of $\tilde{V}(\tilde{r}_*)$ is nothing but a centrifugal barrier in $\tilde{r}_*$.

Despite that the leading two terms of the expansion in (2-28) can nicely approximate the potential at the center of the star, it usually produces a discontinuity across the stellar surface. As QNMs are sensitive to discontinuities, we have to adopt another potential $\tilde{V}_{\rm c}(\tilde{r}_*)$ given by

$$\tilde{V}_{\rm c}(\tilde{r}_*) = \frac{l(l+1)}{\tilde{r}_*^2} - \frac{l(l+1)}{\tilde{R}_*^2} + \left(1-\frac{2}{\tilde{R}}\right)\left(\frac{l(l+1)}{\tilde{R}^2} - \frac{6}{\tilde{R}^3}\right), \quad \tilde{r}_* \le \tilde{R}_*, \tag{2-29}$$

where R_* is obtained from (2-27). This potential is similar to the one in (2-28) around $\tilde{r}_* = 0$ and, in addition, is continuous across the stellar surface. This scheme is termed the centrifugal barrier approximation (CBA) in our paper. It is worthwhile to note that under CBA the wave function of NSRWE inside the star is simply given by $\tilde{k}\tilde{r}_* j_l(\tilde{k}\tilde{r}_*)$, e.g. for $l = 2$:

$$\tilde{\psi}(\tilde{r}_*) = \frac{3\sin(\tilde{k}\tilde{r}_*)}{\tilde{k}^2\tilde{r}_*^2} - \frac{3\cos(\tilde{k}\tilde{r}_*)}{\tilde{k}\tilde{r}_*} - \sin(\tilde{k}\tilde{r}_*), \quad \tilde{r}_* \le \tilde{R}_*. \tag{2-30}$$

Here

$$\tilde{k} = \left[\tilde{\omega}^2 + \frac{l(l+1)}{\tilde{R}_*^2} - \left(1-\frac{2}{\tilde{R}}\right)\left(\frac{l(l+1)}{\tilde{R}^2} - \frac{6}{\tilde{R}^3}\right)\right]^{1/2} \tag{2-31}$$

is the scaled effective wave number.

In addition to its simplicity, as shown in Fig. 1, CBA also yields QNMs (denoted by the solid line in the figure) close to those of TVIIM and realistic neutron stars. Therefore, QNMs of CBA manifest the universal behavior (1-3). This remarkable discovery is indeed the crux of the present paper. As the scaled potential in (2-29) is completely characterized by $\tilde{R} = 1/\mathcal{C}$ and $\tilde{R}_*$, which is also a function of $\mathcal{C}$, the cause of the observed universality in neutron star axial pulsations then becomes obvious and understandable. In a nutshell, the universality is attributable to (i) the centrifugal potential at the center of the star; (ii) the continuity of the potential; and (iii) the tortoise radius $\tilde{R}_*$ of TVIIM star.

3. Scaled-Coordinate Logarithmic Perturbation

After locating the physical origin of the universality in QNMs of neutron stars, we further consider the following questions: (i) Can the coefficients a, b and c in (1-3) be obtained analytically from CBA? (ii) Can QNMs of realistic stars be obtained from those of CBA? We hold positive views on these challenging issues. In this paper, we aim to develop a perturbative study to consider how changes in compactness and EOS could affect the frequencies of the QNMs of a star. In fact, the simplicity and generality of CBA directly leads to a feasible perturbative analysis for QNMs of neutron stars and in turn provides appropriate solutions to these two questions.

As discussed above, axial oscillations of neutron stars are described by NSRWE with a potential term dependent on the distribution of energy-mass density and the pressure inside a star. QNMs of these oscillations are the eigen-solution to (2-1) and, in addition, they are regular at the origin and satisfy the outgoing boundary condition at spatial infinity. It is well known that the wave function of QNMs diverges at spatial infinity and is not amenable to standard perturbation theory (see, e.g. Leung et al. 1999). To this end, we will generalize the logarithmic perturbation theory for QNMs, previously formulated by Leung et al. (1997, 1999) to study how the QNMs of a black hole respond to static perturbations such as a static mass shell, to consider QNMs of neutron stars. In this case, the scaled NSRWE (2-8) that makes use of the scaled coordinate $\tilde{r}$ is obviously more amenable to perturbative expansion since outside the star $\tilde{V}(\tilde{r})$ depends only $\tilde{r}$ and is independent of the stellar mass. Therefore, the method developed here is referred to as the Scaled-Coordinate Logarithmic Perturbation Theory (SCLPT). In the subsequent discussion, we will show that shifts in scaled QNM frequencies can be expressed in terms of integrals with finite domains of integration.

3.1. Perturbative expansion

To formulate a perturbative expansion for the QNM frequency, we introduce a formal perturbation parameter, μ, to measure the departure of the stellar configuration from an unperturbed one, which has a scaled circumferential (tortoise) radius $\tilde{R}_0$ ($\tilde{R}_{*0}$), a scaled potential $\tilde{V}_0(\tilde{r}_*)$, and a QNM with a scaled frequency $\tilde{\omega}_0$. Analogous to other perturbation theories, we will assume that the QNM wave function is known. This assumption does not pose any problems to our current study because we will use the CBA potential as the unperturbed system and, as mentioned above, the wave function can be obtained analytically. Besides, $\tilde{R}_{*0}$ and $\tilde{V}_0(\tilde{r}_*)$ can be obtained from (2-27) and (2-29), respectively. The subject of interest in this paper is to obtain the QNM frequency of a perturbed star whose potential function, as a function of $\tilde{r}_*$, can be expressed as:

$$\begin{aligned} \tilde{V}(\tilde{r}_*) &= \tilde{V}_0(\tilde{r}_*) + \Delta\tilde{V} \\ &= \tilde{V}_0(\tilde{r}_*) + \mu\tilde{V}_1(\tilde{r}_*) + \mu^2\tilde{V}_2(\tilde{r}_*) + ... \ , \end{aligned} \tag{3-1}$$

for $\tilde{r}_* \leq \tilde{R}_*(\mu)$. Here $\tilde{R}(\mu)$ and $\tilde{R}_*(\mu)$ are the circumferential and tortoise radii of the perturbed star, respectively, which are also functions of μ, with $\tilde{R}(\mu = 0) = \tilde{R}_0$ and $\tilde{R}_*(\mu = 0) = \tilde{R}_{*0}$.

Outside the star, it is clear from (2-9) that $\tilde{V}$, as a function of $\tilde{r}$, is independent of μ and hence $\Delta\tilde{V} = 0$ for $\tilde{r} \geq \tilde{R}(\mu)$. It is therefore more convenient to adopt the scaled tortoise coordinate $\tilde{r}_*$ and the scaled circumferential radius $\tilde{r}$ to describe wave propagation inside and outside the star, respectively. Each of these radial coordinates has its own advantage. The scaled tortoise coordinate description casts the NSRWE into the standard Klein-Gordon equation form, whereas the use of the scaled circumferential radius simplifies the form of $\tilde{V}$ outside the star. In our formalism, we will apply these coordinates in different regions of interest.

In the following we seek a power series expansion for the QNM frequency $\tilde{\omega}(\mu)$ of the perturbed star:

$$\tilde{\omega}(\mu) = \tilde{\omega}_0 + \mu\tilde{\omega}_1 + \mu^2\tilde{\omega}_2 + ... \ . \tag{3-2}$$

We will find a general expression for $\tilde{\omega}_n$ ($n = 1, 2, 3, ...$) and explicitly determine the leading two expansion coefficients, $\tilde{\omega}_1$ and $\tilde{\omega}_2$.

3.2. Connection formula

Inside the star we adopt the scaled tortoise coordinate $\tilde{r}_*$ as the independent variable and consider the solution to (2-8) as a function of three independent variables $\tilde{r}_*$, $\tilde{\omega}$ and μ,

namely:

$$\tilde{\psi} = \tilde{\psi}_-(\tilde{r}_*, \tilde{\omega}, \mu). \tag{3-3}$$

This solution is specified by the regularity condition at the origin and holds for $\tilde{r}_* < \tilde{R}_*$. Outside the star ($\tilde{r} \geq \tilde{R}$), the scaled circumferential radius is used instead and we regard the solution to (2-8) there as a function of $\tilde{r}$ and $\tilde{\omega}$. In particular, $\tilde{\psi}_+(\tilde{r}, \tilde{\omega})$ is a solution that satisfies the outgoing wave boundary condition at spatial infinity. Outside the star, NSRWE is identical to the Regge-Wheeler equation of black holes and therefore $\tilde{\psi}_+(\tilde{r}, \tilde{\omega})$ can be obtained from the Leaver's series solution originally developed for determination of QNMs of black holes (Leaver 1986b; Liu 1997; Leung et al. 1999).

For each μ, we can evaluate the QNM frequency $\tilde{\omega}$ by matching the logarithmic derivatives of $\tilde{\psi}_+$ and $\tilde{\psi}_-$ at $\tilde{r} = \tilde{R}(\mu) = \tilde{R}_0 + \mu\tilde{R}_1 + \mu^2\tilde{R}_2 + \cdots$, i.e.

$$f_-(\tilde{R}_*(\mu), \tilde{\omega}(\mu), \mu) = f_+(\tilde{R}(\mu), \tilde{\omega}(\mu)), \tag{3-4}$$

where

$$f_-(\tilde{r}_*, \tilde{\omega}, \mu) = \frac{1}{\tilde{\psi}_-(\tilde{r}_*, \tilde{\omega}, \mu)} \frac{\partial \tilde{\psi}_-}{\partial \tilde{r}_*}, \tag{3-5}$$

$$\begin{aligned} f_+(\tilde{r}, \tilde{\omega}) &= \frac{1}{\tilde{\psi}_+(\tilde{r}, \tilde{\omega})} \frac{\partial \tilde{\psi}_+}{\partial \tilde{r}_*}, \\ &= \frac{(\tilde{r} - 2)}{\tilde{r}\tilde{\psi}_+(\tilde{r}, \tilde{\omega})} \frac{\partial \tilde{\psi}_+}{\partial \tilde{r}}. \end{aligned} \tag{3-6}$$

It is interesting to note that $f_\pm$ are matched at the scaled radius $\tilde{R}(\mu)$ (or $\tilde{R}_*(\mu)$) that would vary with μ.

3.3. Expansion of logarithmic derivative

To generate an expansion for the QNM frequency $\tilde{\omega}(\mu)$, we firstly expand f_- as a power series in the perturbation parameter μ:

$$f_-(\tilde{r}_*, \tilde{\omega}(\mu), \mu) = f_0(\tilde{r}_*) + \mu f_1(\tilde{r}_*) + \mu^2 f_2(\tilde{r}_*) + \ldots , \tag{3-7}$$

where $f_-(\tilde{r}_*, \tilde{\omega}_0, \mu = 0) = f_0(\tilde{r}_*)$ and we have suppressed the dependence on $\tilde{\omega}_0$ in the expansion coefficients $f_i(\tilde{r}_*)$ ($i = 1, 2, 3, \ldots$). By transforming (2-8) into the form of the Riccati equation:

$$f_-' + f_-^2 + \tilde{\omega}^2 - \tilde{V}(\tilde{r}_*) = 0, \tag{3-8}$$

making use of the expansions (3-1) and (3-2), and comparing equal powers of μ, we show that

$$f_n' + 2f_0 f_n + 2\tilde{\omega}_0\tilde{\omega}_n = \tilde{U}_n, \quad n = 1, 2, \ldots . \tag{3-9}$$

Here $\tilde{U}_1(\tilde{r}_*) = \tilde{V}_1(\tilde{r}_*)$ and for $n \geq 2$,

$$\tilde{U}_n(\tilde{r}_*) = \tilde{V}_n(\tilde{r}_*) - \sum_{i=1}^{n-1}[f_i(\tilde{r}_*)f_{n-i}(\tilde{r}_*) + \tilde{\omega}_i\tilde{\omega}_{n-i}], \tag{3-10}$$

and we have used the prime to symbolize differentiation with respect to $\tilde{r}_*$. Eq. (3-9) can be solved by introducing the integrating factor $\exp[2\int^{\tilde{r}_*} dy f_0(y)] = \tilde{\psi}_0^2(\tilde{r}_*)$, resulting in an integral expression for $f_n(\tilde{R}_{*0})$:

$$f_n(\tilde{R}_{*0})\tilde{\psi}_0^2(\tilde{R}_{*0}) = \int_0^{\tilde{R}_{*0}} \mathrm{d}\tilde{r}_*[\tilde{U}_n(\tilde{r}_*) - 2\tilde{\omega}_0\tilde{\omega}_n]\tilde{\psi}_0^2(\tilde{r}_*). \tag{3-11}$$

Secondly, as the logarithmic derivatives are to be matched at $\tilde{r}_* = \tilde{R}_*(\mu) = \tilde{R}_{*0} + \mu\tilde{R}_{*1} + \mu^2\tilde{R}_{*2} + \cdots$, we expand $f_-(\tilde{R}_*(\mu), \tilde{\omega}(\mu), \mu)$ and $f_+(\tilde{R}(\mu), \tilde{\omega}(\mu))$ in power series of μ, yielding:

$$\begin{aligned} f_-(\tilde{R}_*(\mu), \tilde{\omega}(\mu), \mu) &= f_0(\tilde{R}_*(\mu)) + \mu f_1(\tilde{R}_*(\mu)) + \mu^2 f_2(\tilde{R}_*(\mu)) + ... \\ &= \left[f_0(\tilde{R}_{*0}) + \mu\frac{\mathrm{df_0}}{\mathrm{d}\mu} + \frac{\mu^2}{2!}\frac{\mathrm{d}^2 f_0}{\mathrm{d}\mu^2} + ...\right] \\ &\quad +\mu\left[f_1(\tilde{R}_{*0}) + \mu\frac{\mathrm{d}f_1}{\mathrm{d}\mu} + \frac{\mu^2}{2!}\frac{\mathrm{d}^2 f_1}{\mathrm{d}\mu^2} + ...\right] \\ &\quad +\mu^2\left[f_2(\tilde{R}_{*0}) + \mu\frac{\mathrm{d}f_2}{\mathrm{d}\mu} + \frac{\mu^2}{2!}\frac{\mathrm{d}^2 f_2}{\mathrm{d}\mu^2} + ...\right] + ... , \end{aligned} \tag{3-12}$$

and

$$\begin{aligned} f_+(\tilde{R}(\mu), \tilde{\omega}(\mu)) &= f_+(\tilde{R}(\mu), \tilde{\omega}(\mu)) \\ &= f_+(\tilde{R}_0, \tilde{\omega}_0) + \mu\frac{\mathrm{d}f_+}{\mathrm{d}\mu} + \frac{\mu^2}{2!}\frac{\mathrm{d}^2 f_+}{\mathrm{d}\mu^2} + ... \end{aligned} \tag{3-13}$$

Here it is understood that all derivatives with respective to μ are evaluated at $\mu = 0$. Hence, by comparing equal powers of μ in (3-12) and (3-13), $f_n(\tilde{R}_{*0})$ can be expressed in terms of derivatives of f_i $(i < n)$ and f_+ as follows:

$$\begin{aligned} f_n(\tilde{R}_{*0}) &= \frac{1}{n!}\frac{\mathrm{d}^n f_+}{\mathrm{d}\mu^n} - \left[\frac{1}{n!}\frac{\mathrm{d}^n f_0}{\mathrm{d}\mu^n} + \frac{1}{(n-1)!}\frac{\mathrm{d}^{n-1} f_1}{\mathrm{d}\mu^{n-1}} + \cdots + \frac{\mathrm{d}f_{n-1}}{\mathrm{d}\mu}\right] \\ &= \frac{1}{n!}\frac{\mathrm{d}^n f_+}{\mathrm{d}\mu^n} - \Theta_n, \end{aligned} \tag{3-14}$$

where, by definition, Θ_n is equal to the sum in the square bracket. Furthermore, by introducing another expression Δ_n defined by:

$$\Delta_n = \left[f_+(\tilde{R}_0 + \mu\tilde{R}_1 + \cdots + \mu^{n-1}\tilde{R}_{n-1}, \tilde{\omega}_0 + \mu\tilde{\omega}_1 + \cdots + \mu^{n-1}\tilde{\omega}_{n-1}) - f_+(\tilde{R}_0, \tilde{\omega}_0) \right]_n \quad (3\text{-}15)$$

where $[F(\mu)]_n$ indicates the nth-order term of a function $F(\mu)$, it is readily shown that

$$\frac{1}{n!}\frac{\mathrm{d}^n f_+}{\mathrm{d}\mu^n} = \Delta_n + \left(\tilde{\omega}_n \frac{\partial}{\partial \tilde{\omega}_0} + \tilde{R}_n \frac{\partial}{\partial \tilde{r}} \right) f_+(\tilde{\omega}_0, \tilde{R}_0). \quad (3\text{-}16)$$

As a result, we obtain a formal expansion for the scaled frequency $\tilde{\omega}$, which reads:

$$\tilde{\omega}_n = \frac{\langle \tilde{\psi}_0 | \tilde{U}_n | \tilde{\psi}_0 \rangle}{2\tilde{\omega}_0 \langle \tilde{\psi}_0 | \tilde{\psi}_0 \rangle}, \quad (3\text{-}17)$$

with

$$\langle \tilde{\psi}_0 | \tilde{U}_n | \tilde{\psi}_0 \rangle = \int_0^{\tilde{R}_{*0}} \mathrm{d}\tilde{r}_* \tilde{U}_n(\tilde{r}_*) \tilde{\psi}_0^2(\tilde{r}_*) + \left(\Theta_n - \Delta_n - \tilde{R}_n \frac{\partial f_+}{\partial \tilde{r}} \right) \tilde{\psi}_0^2(\tilde{R}_{*0}), \quad (3\text{-}18)$$

and

$$\langle \tilde{\psi}_0 | \tilde{\psi}_0 \rangle = \int_0^{\tilde{R}_{*0}} \tilde{\psi}_0^2(\tilde{r}_*) \mathrm{d}\tilde{r}_* + \frac{\tilde{\psi}_0^2(\tilde{R}_{*0})}{2\tilde{\omega}_0} \frac{\partial f_+}{\partial \tilde{\omega}_0}. \quad (3\text{-}19)$$

Despite the simplicity of (3-17), which is akin to standard perturbation formulas in quantum mechanics with $\langle \tilde{\psi}_0 | \tilde{\psi}_0 \rangle$ playing the role of the norm squared of a quantum state, the emergence of terms like $\tilde{U}_n$, Δ_n and Θ_n reveals the achievement underlying this formula. It is worthy of remark that in (3-18) there are three different contributions to the frequency shift $\tilde{\omega}_n$, namely an integral over the interior of the star and two surface terms originating from f_+ and f_-, respectively. In the following discussion, we will work out explicit expressions for the first and second order results.

3.4. First and second order frequency shifts

For the case $n = 1$, the expression of $\tilde{U}_1(\tilde{r}_*)$ is trivial, while Θ_n and Δ_n are given by:

$$\Theta_1 = \frac{\mathrm{d}f_0}{\mathrm{d}\mu} = \frac{\mathrm{d}f_0}{\mathrm{d}\tilde{r}_*}\frac{\mathrm{d}\tilde{R}_*}{\mathrm{d}\mu} \quad (3\text{-}20)$$

$$\Delta_1 = 0. \quad (3\text{-}21)$$

As a result, it is clear that

$$\langle \tilde{\psi}_0 | \tilde{U}_1 | \tilde{\psi}_0 \rangle = \int_0^{\tilde{R}_{*0}} \mathrm{d}\tilde{r}_* \tilde{V}_1(\tilde{r}_*) \tilde{\psi}_0^2(\tilde{r}_*) + \left(\tilde{R}_{*1} \frac{df_0}{d\tilde{r}_*} - \tilde{R}_1 \frac{\partial f_+}{\partial \tilde{r}} \right) \tilde{\psi}_0^2(\tilde{R}_{*0}), \quad (3\text{-}22)$$

and hence $\tilde{\omega}_1$ can be readily obtained from (3-17) and (3-19).

For the case $n = 2$, it is straightforward to show that

$$\begin{aligned}
\tilde{U}_2(\tilde{r}_*) &= \tilde{V}_2(\tilde{r}_*) - f_1^2(\tilde{r}_*) - \tilde{\omega}_1^2 \; ; && \text{(3-23)}\\
\Theta_2 &= \frac{1}{2}\frac{\mathrm{d}^2 f_0}{\mathrm{d}\mu^2} + \frac{\mathrm{d}f_1}{\mathrm{d}\mu} \\
&= \frac{\mathrm{d}f_0}{\mathrm{d}\tilde{r}_*}\tilde{R}_{*2} + \frac{1}{2}\frac{\mathrm{d}^2 f_0}{\mathrm{d}\tilde{r}_*^2}\tilde{R}_{*1}^2 + \frac{\mathrm{d}f_1}{\mathrm{d}\tilde{r}_*}\tilde{R}_{*1} \; ; && \text{(3-24)}\\
\Delta_2 &= \left[f_+(\tilde{R}_0 + \mu\tilde{R}_1, \tilde{\omega}_0 + \mu\tilde{\omega}_1) - f_+(\tilde{R}_0, \tilde{\omega}_0)\right]_2 \\
&= \frac{1}{2}\tilde{\omega}_1^2\frac{\partial^2 f_+}{\partial\tilde{\omega}^2} + \tilde{R}_1\tilde{\omega}_1\frac{\partial f_+}{\partial\tilde{r}\partial\tilde{\omega}} + \frac{1}{2}\tilde{R}_1^2\frac{\partial^2 f_+}{\partial\tilde{r}^2}. && \text{(3-25)}
\end{aligned}$$

Direct substitution of these results into (3-18) leads to the second-order term:

$$\begin{aligned}
&\langle\tilde{\psi}_0|\tilde{U}_2|\tilde{\psi}_0\rangle \\
= &\int_0^{\tilde{R}_{*0}} \left[\tilde{V}_2(\tilde{r}_*) - f_1^2(\tilde{r}_*) - \tilde{\omega}_1^2\right]\tilde{\psi}_0^2(\tilde{r}_*)\mathrm{d}\tilde{r}_* \\
&+\tilde{\psi}_0^2(\tilde{R}_{*0})\left[\frac{\mathrm{d}f_0}{\mathrm{d}\tilde{r}_*}\tilde{R}_{*2} + \frac{\tilde{R}_{*1}^2}{2}\frac{\mathrm{d}^2 f_0}{\mathrm{d}\tilde{r}_*^2} + \frac{\mathrm{d}f_1}{\mathrm{d}\tilde{r}_*}\tilde{R}_{*1}\right]_{\tilde{r}_*=\tilde{R}_{*0}} \\
&-\tilde{\psi}_0^2(\tilde{R}_{*0})\left[\frac{\tilde{\omega}_1^2}{2}\frac{\partial^2 f_+}{\partial\tilde{\omega}^2} + \tilde{R}_1\tilde{\omega}_1\frac{\partial f_+}{\partial\tilde{r}\partial\tilde{\omega}} + \frac{\tilde{R}_1^2}{2}\frac{\partial^2 f_+}{\partial\tilde{r}^2} + \tilde{R}_2\frac{\partial f_+}{\partial\tilde{r}}\right]_{\tilde{r}=\tilde{R}_0}, \qquad \text{(3-26)}
\end{aligned}$$

and the second-order frequency change follows directly from (3-17).

After succeeding in deriving the first and second order shifts in the eigenfrequency of QNMs of neutron stars, we will apply relevant formulas to answer the questions posed in the beginning of this section.

4. Universality in QNMs

Being a good global approximation to realistic stars, CBA also demonstrates the universal behavior summarized by (1-3). In fact, the solid line in Fig. 1, representing the QNM frequencies of CBA, is close to the best quadratic fit to those of realistic stars (the dotted line). Therefore, we expect that the universal behavior displayed by realistic neutron stars can be understood from the QNMs of CBA and Eq. (1-3) can be deduced from CBA as well. Motivated by this conjecture, we evaluate the QNM frequency of CBA with SCLPT.

In SCLPT, the QNM frequencies for CBA stars with different compactness can be obtained by considering compactness $\mathcal{C}$ as the perturbation parameter. In this case, the formal expansion parameter $\mu = \mathcal{C} - \mathcal{C}_0$, where $\mathcal{C}_0$ is the compactness of a reference CBA star whose QNMs are known. Hence, to second order in $\mathcal{C} - \mathcal{C}_0$, $\tilde{\omega}(\mathcal{C})$ is approximately given by:

$$\tilde{\omega}(\mu) = \tilde{\omega}_0 + (\mathcal{C} - \mathcal{C}_0)\tilde{\omega}_1 + (\mathcal{C} - \mathcal{C}_0)^2\tilde{\omega}_2\,, \tag{4-1}$$

where $\tilde{\omega}_0$ is the QNM frequency of the reference CBA star. The first and second order shifts in QNM frequencies are proportional to $\mathcal{C} - \mathcal{C}_0$ and $(\mathcal{C} - \mathcal{C}_0)^2$, respectively. Under this approximation, the QNM frequency is expressible in terms of a quadratic function of $\mathcal{C}$:

$$\tilde{\omega} = a\mathcal{C}^2 + b\mathcal{C} + c\,, \tag{4-2}$$

with

$$a = \tilde{\omega}_2; \tag{4-3}$$

$$b = \tilde{\omega}_1 - 2\mathcal{C}_0\tilde{\omega}_2; \tag{4-4}$$

$$c = \tilde{\omega}_0 - \mathcal{C}_0\tilde{\omega}_1 + \mathcal{C}_0^2\tilde{\omega}_2. \tag{4-5}$$

It is obvious that Eq. (4-2) is in prefect agreement with the universal behavior (1-3) discovered numerically by Andersson & Kokkotas (1998); Benhar et al. (1999); Tsui & Leung (2004).

To gauge the accuracy of the second-order SCLPT mentioned above, we apply it to a reference CBA star with compactness $M/R = 0.2$. As shown in Fig. 4, the results obtained from SCLPT (represented by the solid line) are good approximation of the exact QNMs (represented by the stars). This clearly demonstrates the validity of SCLPT. In addition, the perturbative results also faithfully demonstrate the universal behavior displayed by realistic stars (represented by the dotted line), and the numerical values of a, b and c obtained from (4-3),(4-3) and (4-3) respectively are in nice agreement with the those obtained from the best quadratic fit to the QNMs of the realistic stars (see Table 1 for reference). Hence, the universality in axial pulsations of neutron stars is fully understood and predicted analytically.

The technical details of the perturbation scheme yielding $\tilde{\omega}_1$, $\tilde{\omega}_2$ and hence the constants a, b and c are as follows. To obtain the first and second order shifts, we have to evaluate the all quantities appearing in (3-22) and (3-26). Specifically, $\tilde{R}_1$ and $\tilde{R}_2$ are given by:

$$\tilde{R}_1 = \left(\frac{\mathrm{d}\tilde{R}}{\mathrm{d}\mathcal{C}}\right)_{\mathcal{C}=\mathcal{C}_0} = -\frac{1}{\mathcal{C}_0^2}, \tag{4-6}$$

$$\tilde{R}_2 = \frac{1}{2}\left(\frac{\mathrm{d}^2\tilde{R}}{\mathrm{d}\mathcal{C}^2}\right)_{\mathcal{C}=\mathcal{C}_0} = \frac{1}{\mathcal{C}_0^3}. \tag{4-7}$$

Analogously, $\tilde{R}_{*1}$ and $\tilde{R}_{*2}$ can be obtained:

$$\begin{aligned}
\tilde{R}_{*1} &= \left(\frac{\mathrm{d}\tilde{R}_*}{\mathrm{d}\mathcal{C}}\right)_{\mathcal{C}=\mathcal{C}_0} \\
&= \frac{1}{\mathcal{C}_0}\int_0^1 \left[\frac{\partial I(\xi,\mathcal{C}_0)}{\partial \mathcal{C}_0} - \frac{I(\xi,\mathcal{C}_0)}{\mathcal{C}_0}\right]\mathrm{d}\xi, \qquad (4\text{-}8) \\
\tilde{R}_{*2} &= \frac{1}{2}\left(\frac{\mathrm{d}^2\tilde{R}_*}{\mathrm{d}\mathcal{C}^2}\right)_{\mathcal{C}=\mathcal{C}_0} \\
&= \frac{1}{2\mathcal{C}_0}\int_0^1 \left[\frac{\partial^2 I(\xi,\mathcal{C}_0)}{\partial \mathcal{C}_0^2} - \frac{2}{\mathcal{C}_0}\frac{\partial I(\xi,\mathcal{C}_0)}{\partial \mathcal{C}_0} + \frac{2I(\xi,\mathcal{C}_0)}{\mathcal{C}_0^2}\right]\mathrm{d}\xi. \qquad (4\text{-}9)
\end{aligned}$$

On the other hand, as $\tilde{V}_c$ contains explicit dependence on $\tilde{R}_*$ and $\tilde{R}$, $\tilde{V}_1$ and $\tilde{V}_2$ can be found:

$$\begin{aligned}
\tilde{V}_1(\tilde{r}_*) &= \left(\frac{\partial \tilde{V}_c}{\partial \mathcal{C}}\right)_{\mathcal{C}=\mathcal{C}_0} \\
&= \frac{2l(l+1)\tilde{R}_{*1}}{\tilde{R}_{*0}^3} + 2l(l+1)\mathcal{C}_0 - 3(l^2+l+3)\mathcal{C}_0^2 + 12\mathcal{C}_0^3 \\
\tilde{V}_2(\tilde{r}_*) &= \left(\frac{\partial^2 \tilde{V}_c}{\partial \mathcal{C}^2}\right)_{\mathcal{C}=\mathcal{C}_0}, \\
&= -\frac{6l(l+1)\tilde{R}_{*1}^2}{\tilde{R}_{*0}^4} + \frac{4l(l+1)\tilde{R}_{*2}}{\tilde{R}_{*0}^3} + 2l(l+1) - 6(l^2+l+3)\mathcal{C}_0 + 36\mathcal{C}_0^2, \qquad (4\text{-}10)
\end{aligned}$$

which are constants independent of $\tilde{r}_*$.

It is easy to see that $\tilde{V}_n(\tilde{r}_*)$ $(n = 1, 2, 3, \ldots)$ are indeed all $\tilde{r}_*$-independent under CBA. This fact greatly simplifies the perturbation calculation in CBA and renders the integrals involved in the evaluation of $\tilde{\omega}_1$ and $\tilde{\omega}_2$ exactly solvable. For example, noting that $\tilde{\psi}_0(\tilde{r}_*) = \tilde{k}\tilde{r}_* j_l(\tilde{k}\tilde{r}_*)$, we have

$$\int_0^{\tilde{R}_{*0}} \mathrm{d}\tilde{r}_* \tilde{V}_1(\tilde{r}_*)\tilde{\psi}_0^2(\tilde{r}_*) = \frac{\tilde{V}_1\tilde{R}_{*0}}{2}\left\{x^2\left[j_l^2(x) + j_{l-1}^2(x)\right] - (2l+1)xj_l(x)j_{l-1}(x)\right\}_{x=\tilde{k}\tilde{R}_{*0}} \qquad (4\text{-}11)$$

and

$$\begin{aligned}
f_1(\tilde{r}_*) &= \frac{1}{\tilde{\psi}_0^2(\tilde{r}_*)}\int_0^{\tilde{r}_*} \mathrm{d}\tilde{r}'_*[\tilde{V}_1(\tilde{r}'_*) - 2\tilde{\omega}_0\tilde{\omega}_1]\tilde{\psi}_0^2(\tilde{r}'_*) \\
&= \frac{(\tilde{V}_1 - 2\tilde{\omega}_0\tilde{\omega}_1)\tilde{R}_{*0}}{2}\left[1 + \frac{j_{l-1}^2(x)}{j_l^2(x)} - \frac{(2l+1)j_{l-1}(x)}{xj_l(x)}\right]_{x=\tilde{k}\tilde{R}_{*0}}. \qquad (4\text{-}12)
\end{aligned}$$

Besides, we have also apply SCLPT to evaluate QNMs of other realistic stars. As an example, we show here the result for a star constructed with APR2 EOS. As demonstrated in Fig. 5, the second order result of SCLPT is again a good approximation to the exact numerical results. This provides independent corroboration to the validity of SCLPT.

5. Individuality of QNMs

After establishing the universality in axial pulsations of neutron stars, we turn our attention to the individuality of such QNMs. As clearly shown in Figs. 1 and 6, QNM frequencies of individual realistic neutron stars in general deviate slightly from the universal curve (1-3). In the present paper we aim to evaluate QNMs of realistic stars from those of CBA star with SCLPT developed here. For a realistic star whose compactness $\mathcal{C}$ and potential $\tilde{V}(\tilde{r}_*)$ are known, we compare it with a CBA star with the same compactness $\mathcal{C}$. Therefore, we have $\tilde{V}_0 = \tilde{V}_{\rm c}$, $\tilde{V} = \tilde{V}_{\rm c} + \tilde{V}_1$, and $\tilde{R}_* = \tilde{R}_{*0} + \tilde{R}_{*1}$, where $\tilde{R}_{*0}$ is the tortoise radius of the CBA star. However, in this case the scaled circumferential radii of the two stars in consideration are the same. In other words, $\tilde{R}_n = 0$ for $n = 1, 2, \ldots$. Besides, it is convenient to take the formal expansion parameter $\mu = 1$ in the current situation. As both $\tilde{V}_n = 0$ and $\tilde{R}_{*n} = 0$ for $n = 2, 3 \ldots$, the matrix elements $\langle\tilde{\psi}_0|\tilde{U}_1|\tilde{\psi}_0\rangle$ and $\langle\tilde{\psi}_0|\tilde{U}_2|\tilde{\psi}_0\rangle$ can be simplified and respectively take the form:

$$\langle\tilde{\psi}_0|\tilde{U}_1|\tilde{\psi}_0\rangle = \int_0^{\tilde{R}_{*0}} {\rm d}\tilde{r}_* \tilde{V}_1(\tilde{r}_*)\tilde{\psi}_0^2(\tilde{r}_*) + \tilde{R}_{*1}\frac{{\rm d}f_0}{{\rm d}\tilde{r}_*}\tilde{\psi}_0^2(\tilde{R}_{*0}), \tag{5-1}$$

$$\begin{aligned} & \langle\tilde{\psi}_0|\tilde{U}_2|\tilde{\psi}_0\rangle \\ = & -\int_0^{\tilde{R}_{*0}} \left[f_1^2(\tilde{r}_*) + \tilde{\omega}_1^2\right] \tilde{\psi}_0^2(\tilde{r}_*){\rm d}\tilde{r}_* \\ & +\tilde{\psi}_0^2(\tilde{R}_{*0}) \left[\left(\frac{\tilde{R}_{*1}^2}{2}\frac{{\rm d}^2 f_0}{{\rm d}\tilde{r}_*^2} + \tilde{R}_{*1}\frac{{\rm d}f_1}{{\rm d}\tilde{r}_*}\right)_{\tilde{r}_*=\tilde{R}_{*0}} - \frac{\tilde{\omega}_1^2}{2}\left(\frac{\partial^2 f_+}{\partial\tilde{\omega}^2}\right)_{\tilde{r}=\tilde{R}_0}\right]. \end{aligned} \tag{5-2}$$

The first and second order shifts in QNM frequency then follow directly from (3-17), (3-18) and (3-19).

Figure 6 shows QNMs obtained from the perturbation scheme outlined above for stars constructed from various EOSs with a common compactness $\mathcal{C} = 0.20$. The unfilled, dark, and grey symbols respectively indicate the exact, the first and the second order results, while the star is the unperturbed frequency of CBA. It is clearly shown that the second order perturbation results can nicely approximate the exact ones. We have also applied

SCLPT to stable neutron stars with a larger (or smaller) compactness and found that the second-order results are indeed reliable. In fact, the first order formula readily suffices to yield accurate prediction of the shift in $\mathrm{Re}\,\tilde{\omega}$.

On the other hand, we have to point out the limitations of SCLPT. As in other cases, perturbation theory is likely to break down in the presence of instabilities. Therefore, we expect that the accuracy of perturbative results obtained from SCLPT gets worse when the star becomes unstable against perturbation. We verify this point by applying SCLPT to neutron stars constructed with GM24 EOS (Glendenning 1997, p. 244), which are known to be unstable if the compactness is greater than 0.21. As clearly demonstrated in Fig. 7, where QNMs of CBA and GM24 stars with $\mathcal{C} = 0.17, 0.19, 0.20$ are shown, the deviation of the second-order result from the exact value increases as the compactness approaches the border of stability. However, as far as $\mathrm{Re}\,\tilde{\omega}$ is concerned, both the first and second order results are satisfactory.

6. Conclusion and discussion

The main achievement in the present paper is the discovery that the universality in the QNM frequency of axial pulsations of neutron stars in fact originates from the CBA, under which the potential term in the scaled NSRWE is essentially a centrifugal barrier. There are two parameters in the scaled potential, namely the scaled circumferential radius $\tilde{R}$ and tortoise radius $\tilde{R}_*$ of the star. While the former is just the inverse of the compactness $\mathcal{C}$, the latter can be determined from that of TVIIM. These two parameters completely determine the QNMs of CBA and in turn give rise to the observed universality.

In order to consider how the the physical characteristics of a neutron star could affect the frequencies of its QNMs, we have also developed a systematic perturbative scheme SCLPT, which is designed to cope with the divergence in QNM wavefunction at spatial infinity. Direct application of SCLPT to CBA then successfully predicts the universality in the QNM frequency of realistic neutron stars. The advantage of application of the scaled coordinates ($\tilde{r}$ and $\tilde{r}_*$) in our study becomes manifest in this regard because the potential $\tilde{V}$ outside a star is independent of its detailed internal structure save its compactness, leading to the observed universality (Andersson & Kokkotas 1998; Benhar et al. 1999; Tsui & Leung 2004).

On the other hand, SCLPT can also predict small deviations in QNM frequencies from those of CBA for individual realistic neutron stars. This opens possibilities for researchers to link the QNM frequencies observed from a distant star with its internal structure and EOS as well. We are currently working on the inverse problem of SCLPT, namely inferring the

internal structure of a pulsating neutron star from its gravitational wave spectrum. Relevant progress in this direction will be reported elsewhere in due course.

So far we have used the least-damped w-mode to illustrate the principle and accuracy of our method. However, the results mentioned in the present paper are general and hold for modes of higher orders (i.e. modes with frequencies higher than that of the least-damped one). More interestingly, we note that the $w_{\rm II}$-mode (see e.g. Kokkotas & Schmidt 1999, and references therein) also displays similar universality. As shown in Fig. 8, where the real and imaginary parts of the scaled QNM frequencies of the $w_{\rm II}$-modes of various realistic stellar models, TVIIM and CBA are plotted against the compactness, the universality summarized in (1-3) is clearly exhibited. It is remarkable that the corresponding values obtained from application of second-order SCLPT to CBA (the solid line) successfully capture the essence of such universal behavior. To further examine the validity of CBA and SCLPT in this case, we show in Fig. 9 the scaled QNM frequency of a $w_{\rm II}$-mode of a CBA star (the star symbol) and other realistic stars (the unfilled symbols) with a common compactness $\mathcal{C} = 0.2$, the first and second order results obtained from applying SCLPT to the CBA star (respectively denoted by the corresponding dark and grey symbols). It is obvious that SCLPT can indeed reproduce accurate eigenfrequencies for the $w_{\rm II}$-mode.

Despite that we have demonstrated here the validity of CBA and SCLPT for ordinary w-modes and $w_{\rm II}$ modes; we have to caution that the trapped mode is an exception to our method. As is well known, trapped modes usually exist in ultra-compact stars with compactness greater than 1/3 and have small decaying rates (Chandrasekhar & Ferrari 1991b). The physical origin of such modes is the development of a local minimum in the potential $V(r_*)$ inside the star when $\mathcal{C} > 1/3$. Hence, gravitational waves are trapped in the potential minimum and acquire much longer lifetime. The analysis proposed in the present paper relies on the validity of the CBA model whose potential term $V(r_*)$ is obviously a monotonic function inside the star. In fact, the CBA potential deviates significantly from those of TVIIM (or other ultra-compact stars). As shown in Fig. 10, trapped modes of CBA are no longer good approximation to those of TVIIM if $\mathcal{C} > 1/3$ and therefore it is not possible to obtain the trapped modes of TVIIM (or other ultra-compact stars) from application of SCLPT to CBA. We conclude our paper with this remark.

We thank J Wu for discussions. We also express our gratitude to an anonymous referee for drawing our attention to the $w_{\rm II}$ and the trapped modes. Our work is supported in part by the Hong Kong Research Grants Council (grant No: CUHK4282/00P and 401905) and a direct grant (Project ID: 2060260) from the Chinese University of Hong Kong.

REFERENCES

Akmal, A., Pandharipande, V. R., & Ravenhall, D. G. 1998, Phys. Rev. C, 58, 1804

Alcock, C., Farhi, C. E., & Olinto, A. 1986, ApJ, 310, 261

Andersson, N., & Kokkotas, K. D. 1996, Phys. Rev. Lett., 77, 20

—. 1998, MNRAS, 299, 1059

Belczynski, K., Kalogera, V., & Bulik, T. 2001, ApJ, 572, 407

Benhar, O., Berti, E., & Ferrari, V. 1999, MNRAS, 310, 797

Chandrasekhar, S., & Ferrari, V. 1991a, Proc. R. Soc. A, 432, 247

—. 1991b, Proc. R. Soc. A, 434, 449

Cheng, K. S., Dai, Z. G., Wei, D. M., & Lu, T. 1998, Science, 280, 407

Ching, E. S. C., Leung, P. T., Suen, W. M., & Young, K. 1996, Phys. Rev. D, 54, 3778

Chodos, A., Jaffe, R. L., Johnson, K., Thorne, C. B., & Weisskopf, V. F. 1974, Phys. Rev. D, 9, 3471

Fryer, C. L., Holz, D. E., & Hughes, S. A. 2002, ApJ, 565, 430

Glendenning, N. K. 1997, Compact Stars - Nuclear Physics, Particle Physics, and General Relativity (Springer, NY)

Hughes, S. 2003, Ann. Phys., 303, 142

Kokkotas, K. D., Apostolatos, T. A., & Andersson, N. 2001, MNRAS, 320, 307

Kokkotas, K. D., & Schmidt, B. G. 1999, Living Rev. Rel., 2, 2

Kokkotas, K. D., & Schutz, B. F. 1986, Gen. Relativ. Gravitation, 18, 913

Lattimer, J. M., & Prakash, M. 2001, ApJ, 550, 426

Leaver, E. W. 1986a, Phys. Rev. D, 34, 384

—. 1986b, J. Math. Phys., 27, 1238

Leung, P. T., Liu, Y. T., Suen, W. M., Tam, C. Y., & Young, K. 1997, Phys. Rev. Lett., 78, 2894

—. 1999, Phys. Rev. D, 59, 044034

Lindblom, L. 1992, ApJ, 398, 56

Lindblom, L., Owen, B. J., & Morsink, S. M. 1998, Phys. Rev. Lett., 80, 4843

Liu, Y. T. 1997, MPhil thesis, The Chinese University of Hong Kong

Mason, J. W., ed. 2004, Astrophysics Update, Vol. I (Springer-Praxis), 281–310

Nollert, H.-P. 1999, Class. Quantum Grav., 16, R159

Pandharipande, V. 1971a, Nucl. Phys A, 174, 641

—. 1971b, Nucl. Phys A, 178, 123

Prakash, M., Baron, E., & Prakash, M. 1990, Phys. Lett. B, 243, 175

Press, W. H. 1971, ApJ, 170, L105

Regge, T., & Wheeler, J. A. 1957, Phys. Rev., 108, 1063

Thorne, K. S., & Campolattaro, A. 1967, ApJ, 149, 591

Tolman, R. C. 1939, Phys. Rev., 55, 364

Tsui, L. K., & Leung, P. T. 2004, MNRAS, 357, 1029

Wiringa, R. B., Fiks, V., & Fabrocini, A. 1988, Phys. Rev. C, 38, 1010

Witten, E. 1984, Phys. Rev. D, 30, 272

This preprint was prepared with the AAS LaTeX macros v5.2.

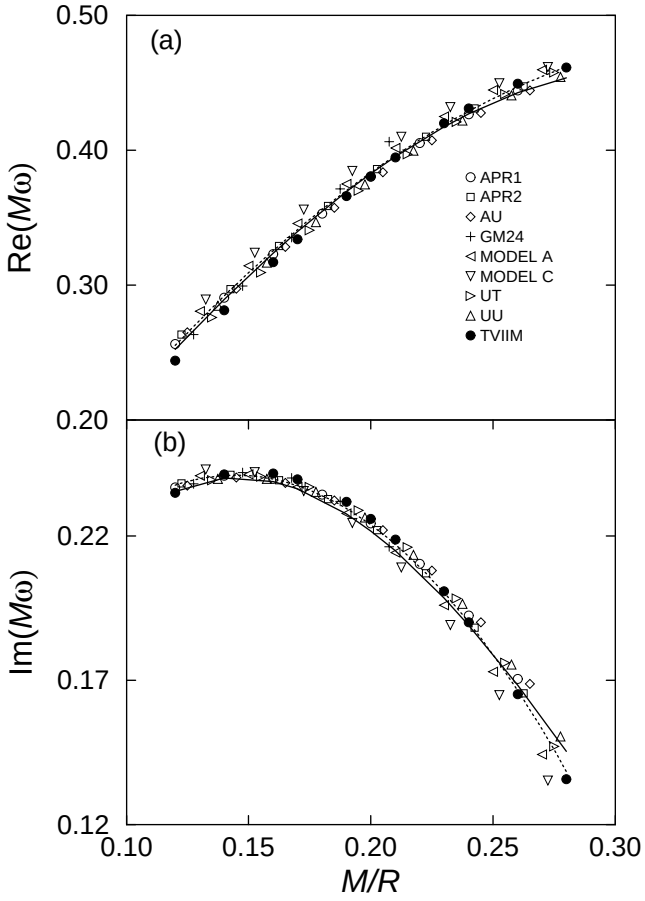

Fig. 1.— The real and imaginary parts of the scaled QNM frequencies of various realistic stellar models (including APR1, APR2, AU, GM24, Models A and B, UT and UU), TVIIM and CBA (solid line) are plotted against the compactness. The dotted line is the best quadratic fit to those of the realistic stars

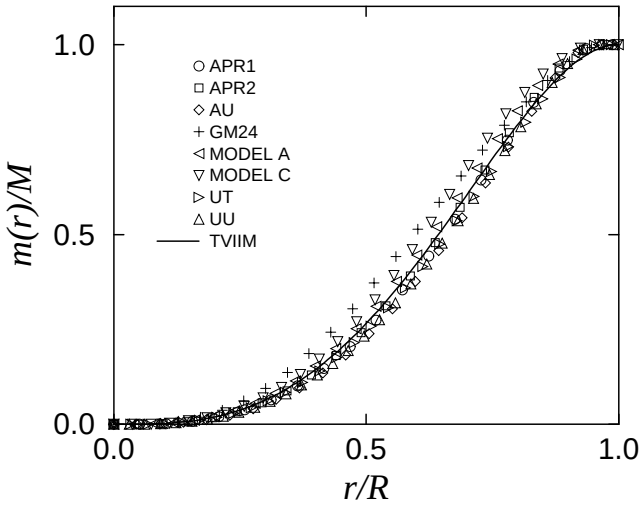

Fig. 2.— The mass distributions of various realistic neutron stars and TVIIM with a common compactness $\mathcal{C} = 0.2$ are plotted against r/R.

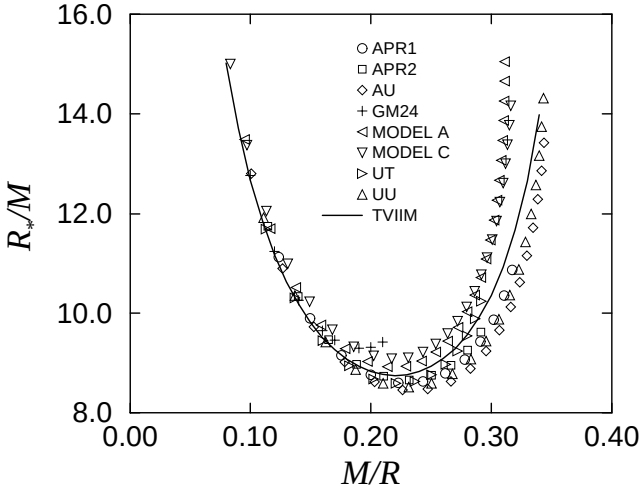

Fig. 3.— The figure shows the relationship between R_*/M and the compactness for TVIIM (solid line) and other realistic neutron stars.

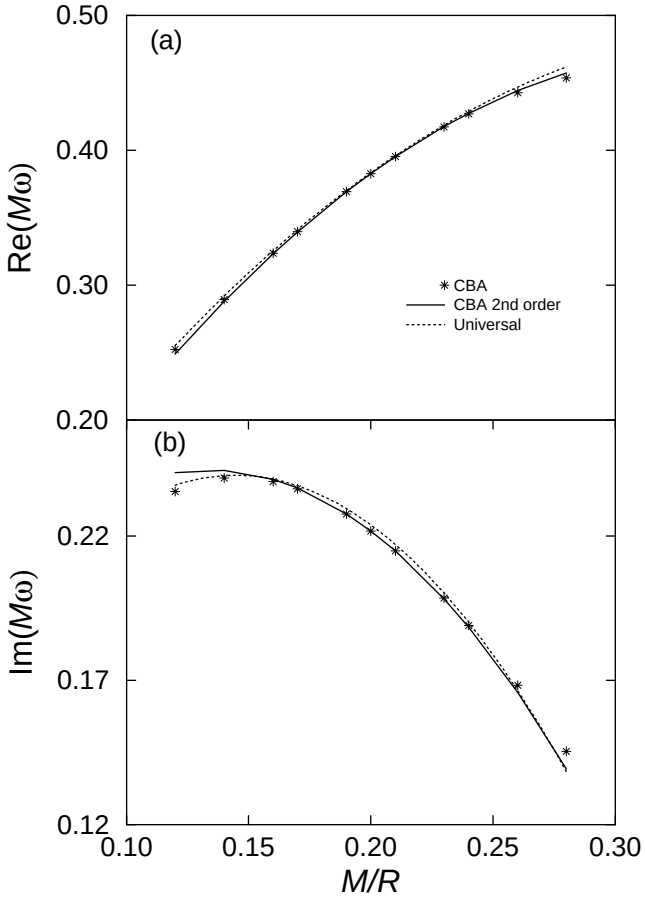

Fig. 4.— The scaled QNM frequency of the CBA star is plotted against the compactness $\mathcal{C}$. The stars and the solid line represent the exact values and the ones obtained from applying the second-order SCLPT to a CBA star with $\mathcal{C} = 0.2$, respectively. For purpose of comparison, we also show the universal curve (the dotted line), i.e. the best quadratic fit to QNM frequencies of the realistic stars considered in this paper.

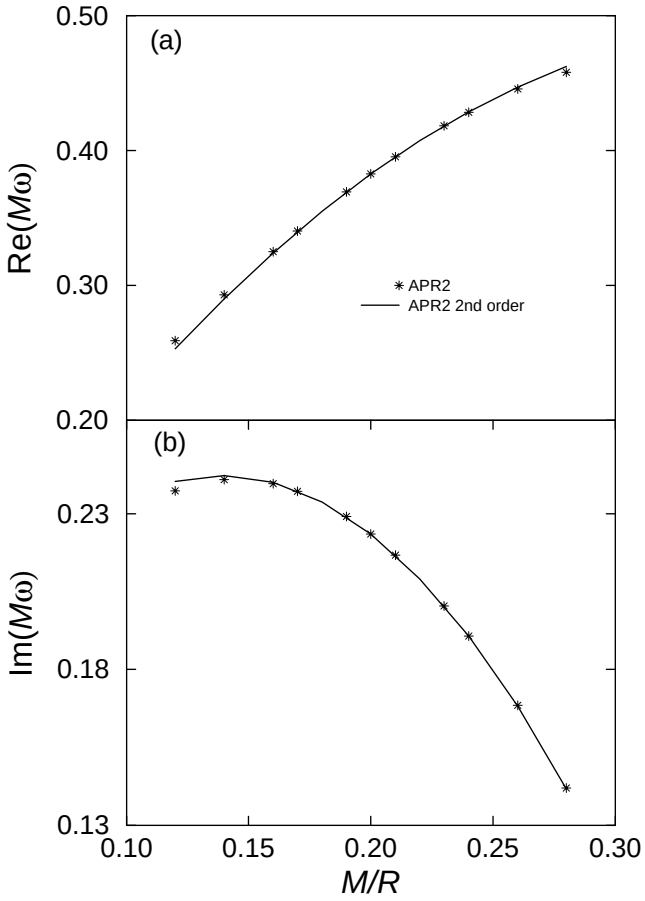

Fig. 5.— The scaled QNM frequency of the APR2 star is plotted against the compactness $\mathcal{C}$. The stars and the solid line are the exact values and the ones obtained by applying the second-order SCLPT to an APR2 star with $\mathcal{C} = 0.2$, respectively.

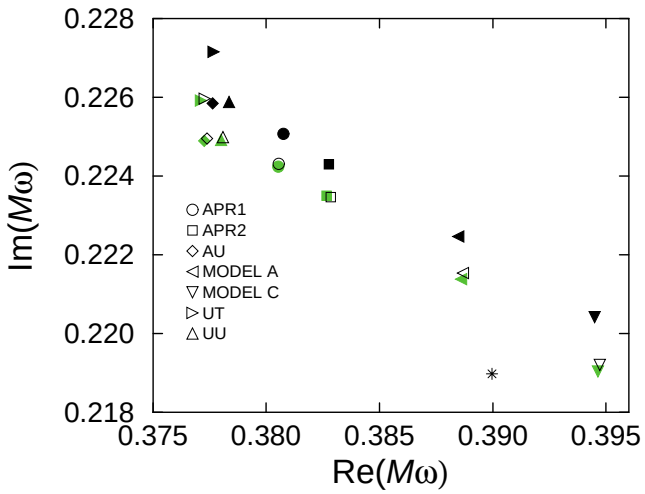

Fig. 6.— The star symbol shows the scaled QNM frequency of a CBA star with compactness $\mathcal{C} = 0.2$. By applying SCLPT to the CBA star, the first and second order results, respectively denoted by dark and grey symbols, for QNM frequencies of realistic stars with the same compactness are obtained. For comparison, exact numerical QNM frequencies of realistic stars are indicated by the corresponding unfilled symbols.

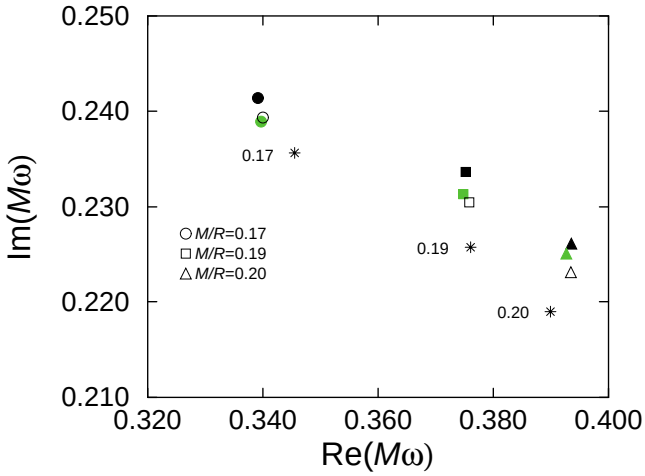

Fig. 7.— The figure shows the scaled QNM frequencies of GM24 stars with $\mathcal{C} = 0.17, 0.19, 0.20$. The star symbol indicates the QNM frequencies of the corresponding CBA stars. The first and second order results obtained from SCLPT are denoted by dark and grey symbols, respectively. For comparison exact numerical QNM frequencies of GM24 stars are indicated by the corresponding unfilled symbols.

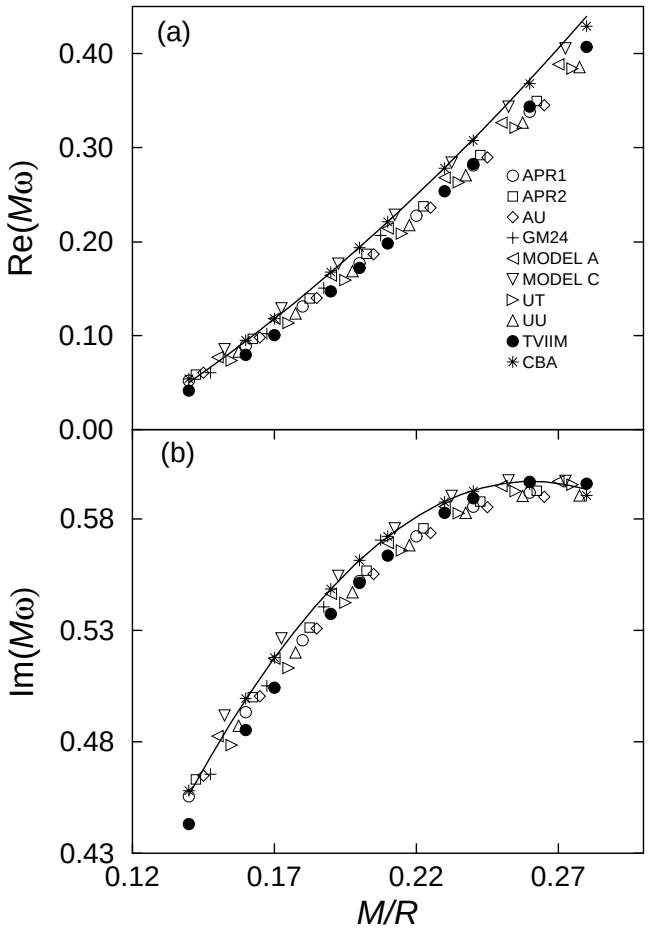

Fig. 8.— The real and imaginary parts of the scaled QNM frequencies of a $w_{\rm II}$-mode of various realistic stellar models, TVIIM and CBA are plotted against the compactness. The solid line shows the corresponding values obtained from the second-order SCLPT.

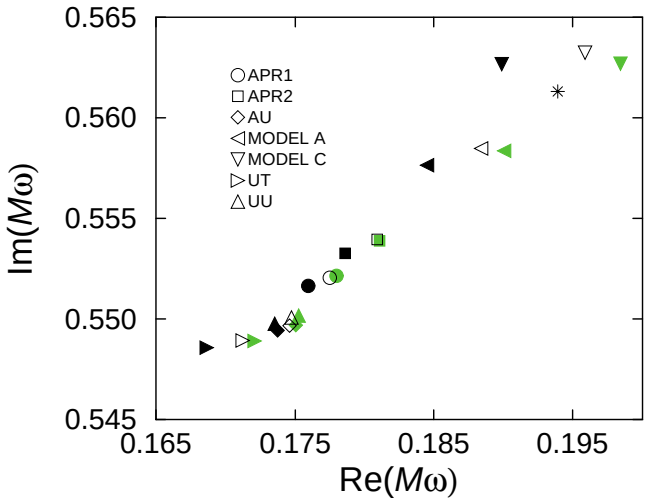

Fig. 9.— The star symbol shows the scaled QNM frequency of a $w_{\rm II}$-mode of a CBA star with compactness $\mathcal{C} = 0.2$. By applying SCLPT to the CBA star, the first and second order results, respectively denoted by dark and grey symbols, for QNM frequencies of realistic stars with the same compactness are obtained. For comparison, exact numerical QNM frequencies of realistic stars are indicated by the corresponding unfilled symbols.

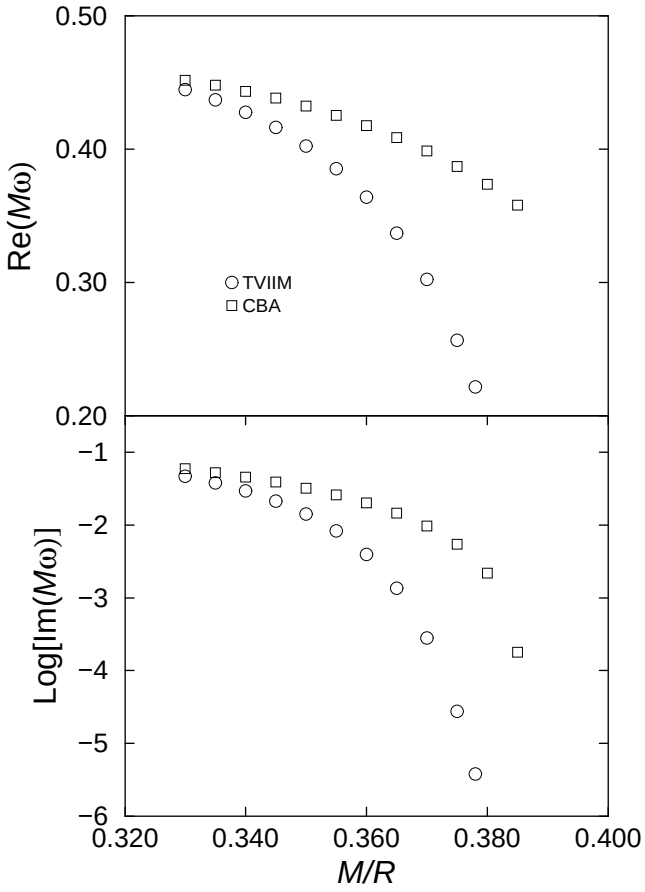

Fig. 10.— The real and imaginary parts of the scaled QNM frequencies of a trapped-mode of TVIIM and CBA are plotted against the compactness.

Data	a	b	c
Best fit to realistic stars	$-3.9 - \mathrm{i}5.6$	$2.8 + \mathrm{i}1.6$	$-0.03 + \mathrm{i}0.125$
Perturbative result of CBA	$-4.63 - \mathrm{i}4.86$	$3.15 + \mathrm{i}1.30$	$-0.063 + \mathrm{i}0.155$

Table 1: The complex coefficients a, b and c in (1-3) are shown. In the first row the values are obtained from the best quadratic fit to the QNMs of the realistic stars considered in Fig. 1, while in the second row those obtained from the second order result of SCLPT for a reference CBA star with compactness $M/R = 0.2$ are presented.